Journal Name

ARTICLE

An experimental and computational framework for engineering multifunctional nanoparticles: designing selective anticancer therapies

Received 00th January 20xx,
Accepted 00th January 20xx

DOI: 10.1039/x0xx00000x

www.rsc.org/

A. Aires,[a,b] J. F. Cadenas,[b] R. Guantes,[c*] and A. L. Cortajarena[a,b,d*]

A key challenge in the treatment of cancer with nanomedicine is to engineer and select nanoparticle formulations that lead to the desired selectivity between tumorigenic and non-tumorigenic cells. To this aim, novel designed nanomaterials, deep biochemical understanding of the mechanisms of interaction between nanomaterials and cells, and computational models are emerging as very useful tools to guide the design of efficient and selective nanotherapies. This works shows, using a combination of detailed experimental approaches and simulations, that the specific targeting of cancer cells in comparison to non-tumorigenic cells can be achieved through the custom design of multivalent nanoparticles. A theoretical model that provides simple yet quantitative predictions to tune the nanoparticles targeting and cytotoxic properties by their degree of functionalization is developed. As a case study, a system that included a targeting agent and a drug and is amenable to controlled experimental manipulation and theoretical analysis is used. This study shows how at defined functionalization levels multivalent nanoparticles can selectively kill tumor cells, while barely affecting non-tumorigenic cells. This work opens a way to the rational design of multifunctionalized nanoparticles with defined targeting and cytotoxic properties for practical applications.

Introduction

Nanomedicine has given rise to an increasing interest in the design and use of nanomaterials for biomedical applications, including cancer treatment.[1-4] Nanoparticles (NP) targeted to surface receptors overexpressed in certain tumours are promising for selective anticancer therapies.[5, 6] A key principle of such strategy is the proper design of NP size and functionalization to selectively discriminate between tumorigenic and non-tumorigenic cells based on a threshold in receptor concentration.[7-12] One possibility to achieve selective targeting against tumorigenic cells is multivalency.[7, 12-14] In this approach, a particle uses multiple ligands to bind simultaneously to several of the receptors displayed on the cell surface. Multivalent ligands often possess increased functional affinity for their targets compared to that of monovalent ligands,[13, 15] and this increased affinity might critically depend on receptor and cell densities. [8, 16]

The application of these principles to specific malignancies requires both a fine experimental control of the functionalization methodologies[17-19] to fabricate NP with the required amounts of targeting ligands and cytotoxic drugs, and quantitative determination of differential NP uptake and cytotoxic effects on both non-tumorigenic and tumorigenic cells under comparable conditions. Mathematical modelling along with quantitative experimentation can provide the necessary knowledge to predict and guide the engineering of nanoformulations better suited for particular treatments. [7, 20-22]

Recent experimental results show that the multivalent pseudopeptide Nucant-6L (N6L) efficiently targets tumorigenic cells and exhibits antitumor activities.[14, 23-26] N6L is a synthetic ligand of cell-surface nucleolin, which shows increased expression in various tumor cell lines and is a marker of several human cancers such as colorectal, lung, cervical and breast carcinomas, melanoma and glioblastoma.[26] N6L system is a relevant model since has been recently shown to inhibit the growth of several types of tumors.[25, 27-29] Additionally, N6L use in nanomedicine approaches was shown to be effective *in*

[a] *CIC biomaGUNE, Paseo de Miramón 182, 20014 Donostia-San Sebastian, Spain.*
[b] *iMdea-Nanociencia, Campus Universitario de Cantoblanco, 28049 Madrid, Spain; Nanobiotecnología (iMdea-Nanociencia), Unidad Asociada al Centro Nacional de Biotecnología (CNB-CSIC), 28049 Madrid, Spain.*
[c] *Department of Condensed Matter Physics, Material Science Institute "Nicolás Cabrera" and Institute for Condensed Matter Physics (IFIMAC), Facultad de Ciencias, Universidad Autónoma de Madrid, Cantoblanco, 28049 Madrid, Spain.*
[d] *Ikerbasque, Basque Foundation for Science, Mª Díaz de Haro 3, E-48013 Bilbao, Spain.*
* *E-mail: alcortajarena@cicbiomagune.es; raul.guantes@uam.es.*

Electronic Supplementary Information (ESI) available: **Model description. Table S1.** Model Parameters and Constants: Definitions and estimated/fitted values. **Figure S1.** TEM images of BSA-NPs. **Figure S2.** Stability of BSA-NPs. **Figure S3.** Release kinetics of the different nanoparticles used. **Figure S4.** Prussian blue staining of cellular uptake in MCF-10A. **Figure S5.** Cellular localization of the different nanoparticles used in MDA-MB-231 and MCF-10A breast cancer cell lines. **Figure S6.** Number of NP internalized by MDA-MB-231 cells. **Figure S7.** Color contour plot of total receptor number R_T in tumorigenic cells as a function of the endocytic and unbinding constants k_e and k_{off}. **Figure S8**. Avidity, calculated from eq. (S17) for the tumorigenic cell line (MDA-MB-231) and for the non-tumorigenic cell line (MCF-10A). **Figure S9.** Internalization of NP in MDA-MB-231 cells, after 5h of incubation with two different formulations (BSA-NP and BSA-NP-N6L_3).
See DOI: 10.1039/x0xx00000x

vitro[26] and *in vivo.*[24] To understand how multivalency can achieve the desired selectivity against tumoral cells and under which conditions in receptor concentration and ligand dose, we have undertaken a quantitative experimental and theoretical investigation of the internalization and effect on cell viability of magnetic iron oxide NP functionalized with the ligand N6L and the cytotoxic drug gemcitabine (GEM). This formulation is directed against normal breast epithelial cells (MCF-10A line) and breast carcinoma cells (MDA-MB-231 line). We first characterize experimentally the amount of internalized NP in tumorigenic and non-tumorigenic breast cells at different doses of the pseudopeptide N6L. These studies reveal that in a situation with more than one ligand attached per NP, internalization is favoured in the tumor cells. These data, together with internalization measurements at different concentrations of NP, are used to calibrate a kinetic model of NP binding and uptake in both cell lines, which captures the effect of differential internalization due to multivalent binding with a minimal set of parameters.

Next, we characterize the viability of the two cell lines after treatment with different cytotoxic formulations (GEM in solution, NP functionalized with GEM, and NP functionalized with GEM and N6L) at different NP concentrations. Our results show that only the formulation with gemcitabine and multivalent N6L attached to NP selectively kills tumor cells, while barely affecting non-tumorigenic cells, consistent with the internalization data. The correspondence between NP uptake and cell survival can be used within the mathematical model to infer the optimal combinations of N6L dose and NP concentrations that allow selective killing of tumor cells.

Results and discussion

Multifunctionalization of NP

In order to perform a systematic experimental study combined with computational modelling it is fundamental to produce custom nanoformulations in which the different components can be precisely modulated, including the number of targeting and cytotoxic agents per nanoparticle. Previous development of functionalization methodologies provides us with the necessary tools to achieve this goal.[24, 30, 31] The general strategy followed to synthesize multifunctional iron NP is sketched in Figure 1. First, bovine serum albumin (BSA) used for biocompatibility is immobilized onto the NP surface.[32] Then, to obtain BSA-NP-GEM, BSA-NP-N6L and BSA-NP-GEM-N6L, the primary amine groups of BSA were modified with sulfhydryl groups using 2-iminothiolane and a gemcitabine derivative was reacted with the activated BSA-NP.[19]

The functionalization of BSA-NP with N6L pseudopeptide was achieved by the formation of disulfide bonds between the reactive thiol of the activated BSA-NP and the activated sulfhydryl groups of N6L derivative.[33] Finally, to obtain the BSA-NP-GEM-N6L formulation, we immobilized the N6L pseudopeptide on BSA-NP-GEM following a protocol previously described.[19, 30, 31] Details are also provided in Methods.

Table 1. Composition and physicochemical properties of the nanoformulations

Nanoformulation	GEM	N6L	ζ (mV)	DH (nm)	PDI
BSA-NP	0 (0)	0 (0)	-29 ± 2	48 ± 1	0.22
BSA-NP-GEM	5 (22)	0 (0)	-26 ± 2	52 ± 1	0.21
BSA-NP-N6L_1	0 (0)	0.25 (1)	-26 ± 1	53 ± 1	0.20
BSA-NP-N6L_2	0 (0)	0.50 (2)	-23 ± 2	60 ± 1	0.23
BSA-NP-N6L_3	0 (0)	1.0 (4)	-21 ± 2	65 ± 2	0.23
BSA-NP-N6L_4	0 (0)	2.0 (8)	-14 ± 3	74 ± 4	0.40
BSA-NP-GEM-N6L	5 (22)	1.0 (4)	-21 ± 3	65 ± 2	0.23

* GEM: µmol GEM g-1 Fe (GEM molecules / NP), N6L: µmol N6L g-1 Fe (N6L molecules / NP), zeta (ζ)-potential, hydrodynamic diameter (D_H), and polydispersity index (PDI) of the nanoformulations.

The amount of BSA coating, as well as the number of GEM and N6L molecules per NP, are precisely controlled in the final nanoformulations. Physicochemical properties, including zeta-potential and hydrodynamic diameter, of all the nanoformulations used in this work are shown in Table 1. Figure S1 and S2 show the morphological characterization by TEM and the determination of colloidal stability of the nanoformulations, which are stable over long storage time periods.

In order to assess the cytotoxic potential of the BSA-NP-GEM and BSA-NP-GEM-N6L under a reducing environment, GEM release was monitored at 1µM or 1 mM of DTT to mimic the extracellular and intracellular conditions, respectively (Figure S3). These formulations showed a release consistent with previous observations[19]: 96–98% drug release when treated with 1 mM DTT (mimicking intracellular conditions) after 6–8 h while only 3–5% of the cargo was released with 1µM DTT (mimicking the extracellular environment) after 6–8h. These results show that the release of GEM is selective and strongly dependent on the reducing environment, so that it will take place mostly inside the cells and is not affected by the presence of the N6L pseudopeptide.

Determination of the optimum incubation time for the specific targeting of breast cancer cells (MDA-MB-231) with BSA-NP-N6L

To make consistent comparisons between different cell lines and formulations, we first determine the optimum incubation time at which internalization of NP is significant and differences in uptake between the N6L functional and non-functional formulations are noticeable.

Equivalent numbers of *in vitro* cultured MDA-MB-231 cells were treated with BSA-NP or BSA-NP-N6L_3, and the presence of iron revealed using Prussian blue staining (Methods).

Journal Name

ARTICLE

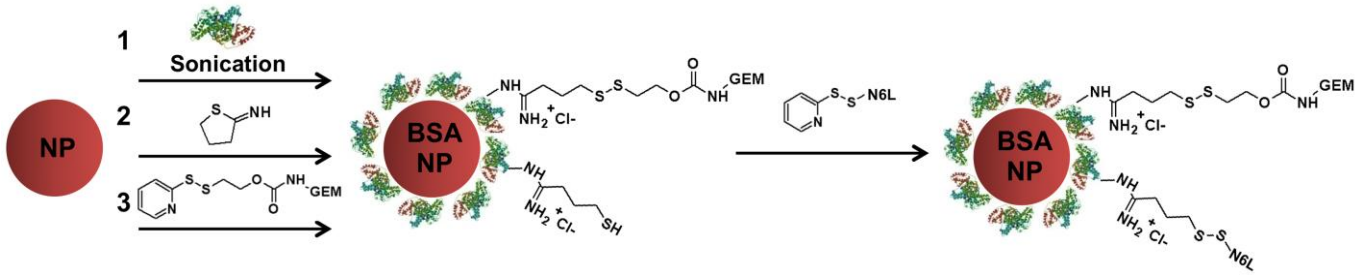

Figure 1. General scheme of the multifunctionalization of NP.

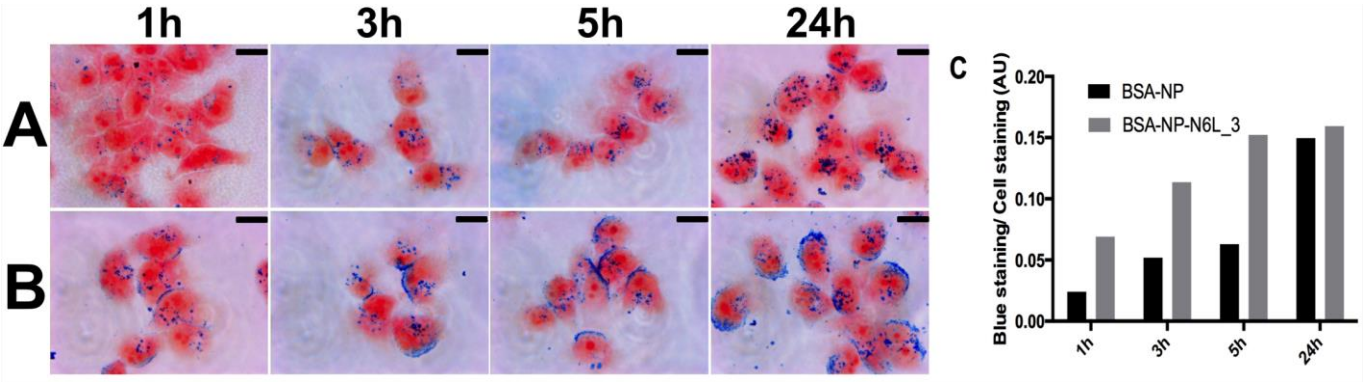

Figure 2. Prussian blue staining of MDA-MB-231 cells incubated with BSA-NP (A) and BSA-NP-N6L_3 (B) for 1, 3, 5 and 24 h at 37ºC (scale bar = 10 µm). C. NP blue staining density values relative to phenol red cell density values expressed in arbitrary units (AU) after 1, 3, 5 and 24 h of treatment with BSA-NP (black bars) BSA-NP-N6L_3 (grey bars).

All Prussian blue cell staining experiments were carried out by incubating MDA-MB-231 cells with BSA-NP or BSA-NP-N6L_3 at an iron concentration of 0.2 mg mL^{-1} for 1, 3, 5 or 24 hours at 37°C. At this concentration, the average number of NP per cell surrounding medium is ~$2.8x10^8$, being in a regime of excess ligand, which facilitates the posterior analysis. As illustrated in Figure 2, the amount of BSA-NP or BSA-NP-N6L_3 localized at the cells increased with incubation time. Although the amount of BSA-NP-N6L in the cells was larger than the BSA-NP at all times, the differences were sharper at short incubation times, as observed previously.[26] This result suggests that cell recognition is more rapid in the presence of N6L. BSA-NP-N6L_3 also displayed remarkably larger accumulation on cell membrane compared to BSA-NP. Based on these results we selected 5 hours as the optimum incubation time to enhance the effect of the specific targeting to breast cancer cells. At this incubation time there is a substantial NP uptake, and the amount of BSA-NP-N6L in the cells is significantly larger compared to BSA-NP. At longer incubation times, the selectivity induced by the presence of the target agent is expected to be negligible.

Intracellular localization of NPs by confocal reflection microscopy

To verify the specific targeting of breast cancer cells (MDA-MB-231) in comparison with non-tumorigenic cells (MCF-10A) with BSA-NP-N6L_3 in the selected conditions, we performed confocal reflection microscopy studies. These allow the visualization of the nanoparticle core at the different confocal planes, ensuring the intracellular localization of the nanoparticles. As illustrated in Figure S5, both BSA-NP and BSA-NP-N6L are internalized and detected in the cytoplasm of the cells. In the case of breast cancer cells (MDA-MB-231), the amount of BSA-NP-N6L localized inside the cells appears significantly larger compared to the BSA-NP. However, in the case of the non-tumorigenic breast cells (MCF-10A) the number of BSA-NP localized in the cells appears larger than the amount of BSA-NP-N6L, in agreement with the Prussian blue experiments shown in Figure S4. These confocal microscopy results confirm the internalization of the NP and the specific targeting of breast cancer cells (MDA-MB-231) in comparison with non-tumorigenic cells (MCF-10A) with BSA-NP-N6L.

Effect of multivalent interactions on NP uptake

To investigate the effect of the number of targeting agents per NP on the specific cell targeting and NP uptake of BSA-NP-N6L for cancer cell lines (MDA-MB-231) in comparison with a non-tumorigenic cell line (MCF-10A), cells were treated with BSA-NP or BSA-NP-N6L (1, 2, 4 and 8 N6L molecules per NP) at 0.2 mg Fe ml^{-1} for 5h, 37°C. After the incubation time, cells were washed and NP internalization was measured on both cell lines by inductively coupled plasma mass spectroscopy (ICP-MS). From the experimental results the number of NP internalized per cell can be quantified as a function of the N6L molecules per NP (Methods). Figure 3 shows with symbols the ICP quantification of internalized NPs for both cell lines. Error bars are standard deviations of three independent measurements.

For non-targeted NP (BSA-NP), internalization is larger in non-tumorigenic cells (MCF-10A). Moreover, the number of internalized NP decreases with increasing N6L dose. This can be attributed to changes in size, nanoparticle aggregation state, surface charge, interaction with cell surface, coating with complement proteins or antibodies, or aggregation.[34] To distinguish these mechanisms from specific binding to N6L receptors, we will use the term non-specific internalization to refer to the internalization of non-targeted NP. For the tumorigenic cell line, functionalization with the N6L pseudopeptide completely reverses the trend, showing an increased internalization with N6L dose (blue circles in Figure 3).

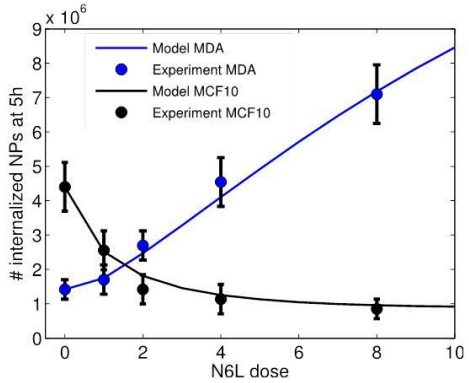

Figure 3. NP internalization at different doses of targeting agent. Symbols: Experimental internalization data measured by ICP-MS of iron NP coated with different doses of the pseudopeptide N6L (without coating, and with 1, 2, 4 and 8 molecules of N6L per NP). Blue: Tumorigenic cell line (MDA-MB-231). Black: Non- tumorigenic cells (MCF-10A). Solid lines are the results of the mathematical model given by equations (1-7). The only specific parameters for the different cell lines are the basal uptake ratio and the number of receptors for N6L (ESI and Table S1).

N6L can specifically bind cell-surface nucleolin, which is overexpressed in various tumor cell lines.[35] N6L can also bind to nucleophosmin,[14] and glycosaminoglycans,[23] both important players in tumor growth and proliferation with increased expression in different tumor malignancies.[36, 37] We thus reason that the large differences observed in NP internalization between tumorigenic and non- tumorigenic cell lines are due to the specific interactions between N6L and proteins overexpressed in the cell membrane of malignant cells.

Multivalent ligand-receptor model of NP binding and internalization

To understand how the concentration of specific surface proteins modulates the internalization of targeted NP, we postulate a simple kinetic model of ligand/receptor binding and internalization that takes into account both specific binding to N6L receptors (nucleolin, glycosaminoglycans…) as well as internalization by other mechanisms and passive uptake. All possible endocytosis mechanisms that do not involve N6L-receptor binding are included in the model as *non-specific* uptake. The multivalent nature of functionalized NP with N6L and the possibility of crosslinking reactions between the NP bound to the cell surface by one or more N6L ligands and the rest of the available ligand sites is included explicitly in the model. [38]

Similar models of multivalent binding have been used in the past to analyse viral attachment to cell surfaces,[39] and antigen recognition by immune cells.[40, 41] Here we generalize the kinetic model of sequential binding of multivalent ligands to cell surface receptors studied by Sulzer and Perelson.[16] Using the law of mass action, the reactions of non-specific uptake, NP association/dissociation to specific cell surface receptors, crosslinking association/dissociation between attached particles and available ligand sites, and NP internalization give the following set of ordinary differential equations:

$$\frac{d\,NP_f}{dt} = -nk_{on}NP_fR + k_{off}C_1 - \alpha_{ns}(N6L)\cdot NP_f \quad (1)$$

$$\frac{d\,C_1}{dt} = nk_{on}NP_fR - k_{off}C_1 - (n-1)k_cC_1R + 2k_{-c}C_2 - k_eC_1 \quad (2)$$

$$\vdots$$

$$\frac{d\,C_i}{dt} = (n-i+1)k_cC_{i-1}R + (i+1)k_{-c}C_{i+1} - [ik_{-c} + (n-i)k_cR]C_i - k_eC_i \quad (3)$$

$$\vdots$$

$$\frac{d\,C_n}{dt} = k_cC_{n-1}R - nk_{-c}C_n - k_eC_n \quad (4)$$

In these equations, NP_f represents the number of free NP per effective volume of medium around a cell. Each NP is coated with n molecules of the N6L ligand, and thus C_i stands for the number of NP per cell bound to the membrane by i ligand sites. R is the number of free specific receptors (for N6L) on the cell surface. The number of free receptors can be obtained from the conservation equation:

$$R_T = R + \sum_{i=1}^{n} i\cdot C_i \quad (5)$$

where R_T is the amount of specific surface receptors per cell, which is assumed to be constant. The experimental readout is the number of internalized NP per cell, that we denote as NP_i. This can be obtained from the conservation of total number of NP per cell medium:

$$NP_i = NP_f^0 - NP_f - \sum_{i=1}^{n} C_i \quad (6)$$

where NP_f^0 is the initial number of free NP per effective cell medium (obtained from experimental conditions). The kinetic rates k_{on} and k_{off} in equation (1) are the binding/dissociation constants of free NP in solution to a specific receptor by one ligand site. Once a NP is attached to the surface, it can bind to another receptor by some available ligand site with crosslinking association and dissociation rates k_c and k_{-c} respectively. All bound NP by *i* ligand sites (C_i, i=1,…,n) can be internalized with an endocytic rate constant k_e. We note that all variables represent numbers of molecules or NP per cell (number of NP per cell surrounding volume in the case of free NP).

The uptake of NP by non-specific mechanisms is effectively taken into account by the last term in equation (1), where the non-specific uptake rate α_{ns} (N6L) depends on both the cell type and the amount of N6L per NP as suggested by the experimental data for the non-tumorigenic MCF-10A cell line in Figure 3. A possible reason for the differences observed in internalization for this cell line, as the N6L dose per NP increases, is that coating with N6L changes charge and surface properties. N6L is positively charged, and increasing N6L dose in NPs can alter the interaction with the culture medium and cell membrane. For instance, adding N6L ligands may change the structure and composition of the protein corona formed around NPs, which impacts on cellular uptake[42]. NPs may also enter cells by passive penetration of the plasma membrane. The ability of NPs to adhere to and penetrate cell membranes was shown to depend on their size and surface charge[43]. On the other hand, iron NPs coated with DMSA have been shown to internalize by a variety of mechanisms, notably by clathrin mediated endocytosis[44]. Receptor mediated endocytosis is dependent on NP size[45], because deformation and wrapping of the cell membrane to form endosomes depends on particle radius[46, 47]. Table 1 shows that increasing the N6L dose increases the hydrodynamic radius of the NPs, and larger particles have longer wrapping times[46], which is consistent with the observation that NP uptake decreases with N6L dose (Figure 3).

Despite the above model contains several simplifications and assumptions (see discussion in Model description, ESI), it is tractable for parameter estimation while taking into account the role of multivalency in functionalized NP. The experimental information about kinetic rate constants in this type of systems is scarce. The main experimentally accessible parameter (for instance, by surface plasmon resonance) is the dissociation equilibrium constant $K_D=k_{off}/k_{on}$. For N6L binding to its specific surface receptors, K_D is in the nanomolar range (K_D ~0.5 nM for nucleolin, ~1 nM for nucleophosmin and ~3-10 nM for glycosaminoglycans.[14, 23] For the dissociation constant, k_{off}, and the endocytosis rate k_e, we can guess only parameter ranges based on similar systems.[20] Since our model can be analytically solved in the cases N6L=0 and N6L=1 (non-functionalized NP and monovalent NP), we use the experimental internalization data in these formulations to estimate the non-specific uptake rate, as well as to constrain parameter values as discussed in ESI text. Details of model calibration, parameter estimation and fitting to experimental results are given in ESI text, Figures S6-S7 and Table S1. We emphasize that our simplified modeling framework is general and can be applied to different cell lines and NP treatments, provided we can measure the number of internalized NP at different ligand doses, and have an estimated value for the dissociation equilibrium constant K_D.

Selective internalization can be solely explained by differences in receptor concentration

With the experimentally estimated or fitted parameters, we numerically solved equations (1-6) (Matlab2014a, MathWorks). Results are shown with solid lines in Figure 3. We note that the same parameters are used for tumorigenic and non-tumorigenic cells, with the only difference of the non-specific uptake constant, α_{ns}, and total number of specific surface receptors, R_T, whose values in both cell lines are constrained by experimental data. In particular, internalization data for the monovalent case (N6L=1) are consistent with at least a 10 fold-change in the amount of specific receptors in the tumorigenic cells compared to the non- tumorigenic ones (ESI and Table S1).

Our data driven model is able to reproduce remarkably well the experimental internalization results of both cell lines in the whole range of N6L doses, considering only differences in the number of specific receptors. This suggests that the multivalent nature of NP binding to surface receptors is the main responsible factor for the selective internalization of NP in tumor cells at large N6L doses. The increased affinity by specific receptors with N6L dose can be rationalized using the concept of 'avidity' or 'effective affinity'.[13, 38] The avidity can be used to characterize the binding of multivalent ligands describing the process as an 'effective' monovalent binding. Within the present model, we can calculate analytically the avidity,[16] which shows that the affinity is increased by ~2,000 in the tumor cell line for the largest N6L dose employed (N6L=8) (ESI and Figure S8).

Selective cell killing by targeted multivalent NP

The ultimate goal of NP functionalization is to achieve maximum efficiency of cell killing of tumoral cells without affecting surrounding healthy cells. It is expected that the greater the number of internalized NP functionalized with a cytotoxic drug, the higher the probability of cell killing, but this correspondence is not necessarily linear and may be different in tumorigenic and non-tumorigenic cells. Thus, the mapping between the amount of internalized NP and cell survival needs to be accurately characterized to design optimal strategies for selective cell killing.

We first performed a series of experiments to measure cell survival using different NP formulations and drug doses, as a function of time. We treated both non-tumorigenic and tumorigenic cell lines with: 1) Gemcitabine free drug in solution at different concentrations (250 nM, 375 nM, 500 nM, 750 nM and 1 μM); 2) Functionalized NP (BSA-NP-GEM) with 22 molecules of gemcitabine per NP, at doses to reach equivalent drug concentrations (0.05, 0.075, 0.1, 0.15 and 0.2 mg Fe ml^{-1}); 3) Functionalized NPs with gemcitabine and 4 molecules of N6L per NP (BSA-NP-GEM-N6L) at the same

doses. To study cytotoxicity in vitro, BSA-NP-N6L_3 formulation was selected as the best trade-off between large selective internalization in the tumor cell line, Figure 3, and colloidal stability of the NP formulation. Production of stable targeted NP with high doses of N6L molecules involves a major experimental challenge. Since negative charges of BSA-NP are responsible for the repulsion between NP and thus their stability, the introduction of the highly positively charged N6L peptide induces a decrease in the overall charge of the coated NP, lowering their stability. Although increasing the amount of N6L molecules per NP from 4 to 8 produced a substantial increase in NP uptake on breast cancer cells, Figure 3, it also showed a decrease in colloidal stability.

Tumorigenic and non-tumorigenic cell cultures were incubated for 5h with each different formulation, and the fraction of survival cells was quantified 1, 2, 3 and 6 days after treatment (Methods). Results are summarized in Figure 4.

We observe that with free drug in solution, Figure 4A,D, non-tumorigenic cells are preferentially killed. The reason may be that more molecules of gemcitabine are internalized in non-tumorigenic cells, or that they are more sensitive to the drug. With drug attached to non-targeted NP, Figure 4B,E, we still observe a preferential killing of non-tumorigenic cells, especially at high NP concentrations. This result is consistent with the fact that the internalization rate of NP without the N6L ligand is higher in the non-tumorigenic cell line (Figure 3, symbols at N6L=0). When NP are functionalized with N6L (Figure 4C,F), this tendency is reversed: most of the non-tumorigenic cells survive, even at the largest NP concentrations, while survival of tumorigenic cells notably decreases both with time after treatment and NP concentration. This result is also consistent with the internalization data reported in Figure 3: while in non-tumorigenic cells the number of internalized NP decreases with an inverse Michaelis-Menten dependence of N6L valence (black symbols in Fig. 3), in tumorigenic cells NP uptake increases in a monotonic way with N6L dose (blue symbols). Therefore, for N6L per NP ≥2, tumorigenic cells internalize more NP than non-tumorigenic cells.

How sensitive is cell death to the amount of NP internalized? To study this correspondence, we first note that at 6 days after treatment, the survival fraction of cells seems to saturate at intermediate to high NP concentrations in non-tumorigenic cells treated with NP alone, Figure 4B. This means that 5h incubation time is sufficient, at these concentrations, to internalize enough NP to kill as many cells as the free drug in solution, Figure 4A. Then, differences in survival after 6 days with other treatments and concentrations must be mainly due to the number of NP internalized.

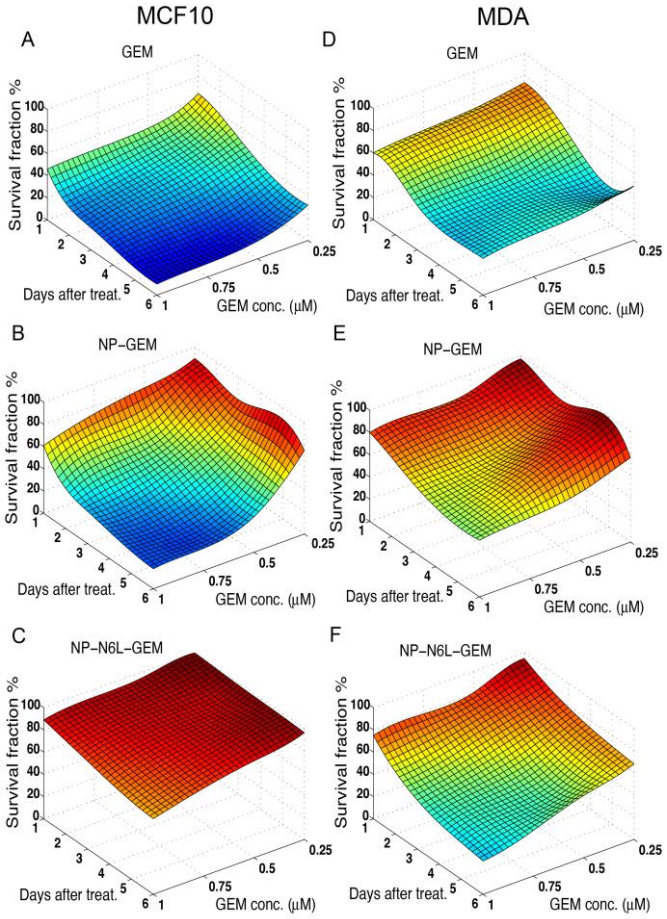

Figure 4. Fraction of survival cells after 5h of incubation with different drug treatments. A, D. Gemcitabine in solution. B, E. Gemcitabine bound to iron NP (BSA-NP-GEM). C, F. Gemcitabine bound to iron NP coated with 4 molecules of N6L (BSA-NP-GEM-N6L). The left column shows the results in non- tumorigenic cells, and the right column in tumorigenic cells.

To check whether there is a one-to-one correspondence between NP internalization and number of cells death after 6 days, we simulated with our fitted mathematical model the number of NP internalized for different NP concentrations in the non-tumorigenic and tumorigenic cell lines, for the experimental BSA-NP-GEM and BSA-NP-GEM–N6L formulations (N6L=0 and N6L=4, respectively). To each simulated value we assign the correspondent survival data extracted from experiment. The model internalization results are plotted against the survival experimental data in Figure 5. We observe that there is a monotonic correspondence between internalization and cell death after 6 days, albeit different for the two cell lines. In ESI, Figure S9, we gather experimental and simulated internalization values in the MDA cell line to show the consistency between the two sets of data.

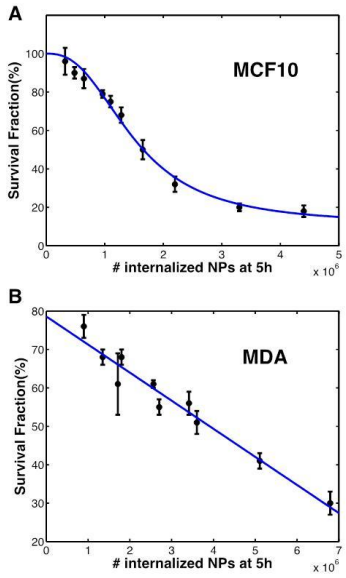

Figure 5. Correspondence between number of NPs internalized per cell (model simulations) and probability of cell death (quantified as the survival fraction of cells at 6 days after treatment, experimental data). A. Non-tumorigenic cell line (MCF-10A). B. tumorigenic cell line (MDA-MB-231). Blue lines are fitting to a sigmoidal function of the form $f(NP_i)=a_0+((100-a_0)/(1+(NP_i/K_s)^n)$ for MCF-10A cells, with parameters a_0=11, K_s=1.5x10^6, n=2.55 and to a straight line $f(NP_i)=a+b\cdot(NP_i)$, with a=78.6, b=7.2x10^{-6} for MDA-MB-231 cells.

The correspondence between uptake and long-term survival can be fitted to simple functional forms (a sigmoid for MCF-10A cells and a straight line for MDA-MB-231 cells, blue lines in Figure 5). These functional forms can be used to predict the fraction of death cells in a wide range of NP concentration and N6L doses for both cell lines, using model simulations, and thus to establish the optimal formulations for selective killing of tumor cells. As an illustration, we define a selectivity index as:

$$s = \frac{P_s^h - P_s^t}{P_s^h + P_s^t} \qquad (7)$$

where P_s stands for survival probability and the superscripts h, t stand for non-tumorigenic and tumorigenic cell lines respectively. Note that this index takes the maximum value s=1 when P_s^h=1, P_s^t=0 (all non-tumorigenic cells survive and all tumorigenic cells are killed, full positive selectivity), and the minimum value s=-1 when P_s^h=0, P_s^t=1 (complete negative selectivity).

Using the model parameters fitted to the internalization data in Figure 3, and the functional correspondence between internalization and survival characterized in Figure 5, we numerically calculate the selectivity index as a function of both NP initial concentration and N6L dose. Results are shown in Figure 6.

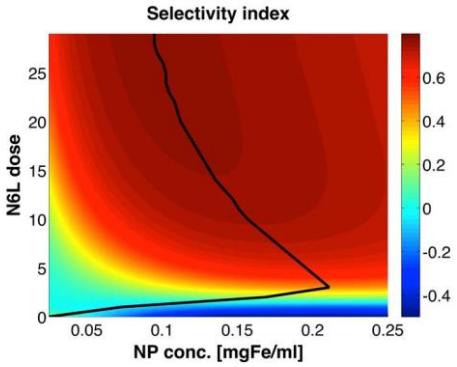

Figure 6. Selectivity index, Eq. (7) as a function of initial NP concentration and number of N6L per NP. The color code corresponding to the selectivity index is shown on the side. The black line marks the initial NP concentration corresponding to the maximum value of selectivity index at each N6L dose.

We notice that for the non-targeted and monovalent formulations selectivity is negative, as already suggested by the experimental results in Figure 6. The larger the available N6L ligands per NP (N6L dose) the larger the selectivity for tumor cell killing. However, we observe that there exists an optimum value in NP concentration for each N6L dose where this selectivity is maximum (black line in Figure 6). While with N6L=4, a concentration of ~0.2 mg Fe ml^{-1} (the conditions used in our experimental study of cytotoxicity) are close to optimal, for larger N6L doses simulations suggest that smaller concentrations could be more favourable for selective killing of cancer cells.

Conclusions

Nanoparticles provide opportunities for designing and tuning properties to optimize therapeutics for specific cancers. The 'ideal' treatment should effectively kill most tumoral cells while showing minimal toxicity to non-tumorigenic cells. In this work we showed how this selectivity can be engineered and optimized using a combination of chemical manipulation and quantitative functionalization of NP, and theoretical modelling. The guiding principle exploits the fact that in most cancer cells there is overexpression of certain receptors. By functionalizing NP with multiple targeting ligands against these receptors, a sharp discrimination in the amount of bound and internalized NP can be achieved between cell surfaces above and below a threshold in receptor concentration.[7] The application of this guiding principle to treat specific malignancies with clinical success requires both quantitative information of the uptake and cytotoxic effects of multivalent NP formulations, and a deeper understanding of the mechanisms originating selective behaviour.

Using chemical manipulation, we have been able to modulate the targeting load of individual iron NP, and different formulations have been tested against non-tumorigenic and

tumorigenic cells under controlled and comparable experimental conditions. These conditions, together with accurate quantification of the number of NP internalized per cell as a function of the ligand dose, allows us to calibrate a kinetic model with the basic ingredients of NP binding, multivalent cross-linking reactions, and internalization. Our modelling framework corroborates that the multivalent nature of targeted NP is responsible for the selectivity in NP uptake observed in the tumorigenic line, and allows an estimation of the fold-change differences in receptor abundance necessary to observe such selective behaviour with the N6L ligand in breast cancer cells.

We have also quantified experimentally the cytotoxic effects of different NP formulations at different drug doses in cancer and non-tumorigenic cells. These data are useful to establish a mapping between the number of NP internalized per cell (the model output) and the experimental cytotoxic effect in tumorigenic and non-tumorigenic cells. This correspondence is relevant to design the ligand dose, drug dose, and concentration of NP that maximize selectivity within a range of attainable experimental conditions. This model can be generally applicable to other nanoformulations including a broad range of targeting agents and drugs, provided we can measure the number of NPs internalized without specific ligand and with different specific ligand doses.

While our model does not account for inhomogeneities in the cell milieu and considers non-specific uptake mechanisms in a phenomenological manner, when used in conjunction with *in vitro* controlled experimental conditions as done here it constitutes a useful first step towards the rational design of the suitable NP doses and formulations for a selective therapy. In clinical or *in vivo* situations, the effect of functionalized NPs on selective cell killing is hard to predict, owing to many complicating factors: the specific characteristics and heterogeneity of the tumor microenvironment and extracellular matrix, NP clearance and vascular extravasation, as well as NP diffusion and tissue penetration.[48] We can envision several extensions of our core kinetic model to account, at least partially, for some of these factors. The most straightforward is taking into account diffusion across tissue cells by adding a diffusion term to our reaction differential equations, as in Hauert et al.[20] A more elaborate possibility that explicitly considers extravasation and clearance of NPs around tumor cells is a multicompartment model, where a compartment representing clearance and transport of NPs in circulating blood is coupled to a different compartment accounting for ligand-receptor binding, internalization and diffusion across the tumor.[49] Finally, our core kinetic model can be combined with multiscale spatial models of tumor growth where cell morphology, cell division and even heterogeneity in the cell population can be taken into account to simulate treatment outcome.[50, 51]

Experimental cell cultured models differ also from *in vivo* systems both in the characteristics of the individual cells[52] and by the multiple factors that hinder tissue penetration and accumulation of NPs around tumor cells. As for the particular system investigated here, the N6L peptide has been successfully used as targeting agent combined with nanomedicine approaches, both in vitro[26] and in vivo.[24, 26] First, in vivo testing in cancer animal models using intratumoral administration showed the efficacy of N6L for intracellular delivery of nanoparticles and ultimately the therapeutic synergy of N6L, a chemotherapeutic drug and hyperthermia treatment.[24] Secondly, systemic administration of NP-N6L nanoformulations resulted in a significant tumor accumulation compared to non functionalized NPs.[26] These results highlight the potential of these approaches to be applied in *in vivo* systems.

Materials and Methods

Materials

Gemcitabine was purchased from Fluorochem. Ultrapure reagent grade water (18.2 MΩ, Wasserlab) was used in all experiments. The non-coated maghemite (Fe_2O_3) NP used in this work, were synthetized by co-precipitation method and supplied by the research group of Dr. Salas at IMDEA Nanociencia.[53, 54] Courty's group from CRRET-CNRS laboratory provided cysteine modified Nucant pseudopeptide (N6L-Cys).[14] Gemcitabine derivative (GEM-S-S-Pyr) and Nucant pseudopeptide (N6L) derivative (Nucant-S-S-Pyr) were prepared according to described procedures.[19]

Multifunctionalization of NP

Synthesis of albumin coated iron oxide NP

First, 235 µL of NP stock at 68 mg Fe mL^{-1} (16 mg of Fe) was added to 30 mL of 10 mM sodium phosphate buffer pH 7.4 (PB buffer) and the NP suspension was shortly vortexed and sonicated (using a J. P. Selecta ultrasonic) for 20 min at room temperature. Then, 667 µL of a bovine serum albumin (BSA) solution (5 mg mL^{-1}) was added to the NP suspension. The reaction mixture was sonicated for 1.5 h in three different cycles, 30 min each. Temperature was controlled in each cycle not to allow temperatures above 35°C that could damage the protein. Once the immobilization is finished, and before BSA excess removal, a sample of 100 µL was separated, mixed with 10 µL of Brine and centrifuged 10 min at 21500 rpm. Supernatant was used for protein concentration measurement using Bradford assay. The amount of immobilized BSA was determined as the difference between the remaining BSA in the supernatant after the immobilization and the BSA concentration initially added to the NP (µg BSA mg^{-1} Fe). Excess of protein, which was not immobilized on the NP, was removed as follows: the reaction mixture was first washed once with PB buffer using a 15 mL filtration unit (10000 MWCO) by centrifugation 5 min at 4500 rpm. Then, the NP were pelleted and washed with PBS removing the supernatant containing BSA excess. NP were finally resuspended in PB to 2 mg Fe mL^{-1} concentration.

BSA-NP activation

8 ml of BSA-NP at 2 mg Fe mL^{-1} were incubated overnight at 37ºC with 150 µmol of 2-iminothiolane g^{-1} Fe. After 16 h, the

sample was washed by 3 cycles of centrifugation and redispersion in PB buffer.

Once the activation finished, and before washing steps, a sample of 100 µL was separated, mixed with 100 µmol of 2-aldrithiol g^{-1} Fe solution and incubated 2 h at 37°C for BSA-NP sulfhydryl group quantification. The sulfhydryl groups added to the BSA-NP were determined by quantification of the 2-pyridinethione released on the reaction between the thiol groups of BSA-NP and the 2-aldrithiol (λmax= 343 nm, ε343nm= 8080 M cm^{-1}).

Covalent attachment of GEM on BSA-NP

8 ml of activated BSA-NP at 2 mg Fe mL-1 were incubated overnight at 37°C with 15 µL of 10 mM GEM derivative (GEM-S-S-Pyr) (7.5 µmol g-1 Fe). After reaction, 20 µL of brine were added and the sample centrifuged 10 min at 21500 rpm. From the collected supernatants, the covalently immobilized GEM onto activated BSA-NP was determined by quantification of the 2-pyridinethione released (λmax= 343 nm, ε343nm=8080 M cm^{-1}). Finally, the sample was redispersed in 8 mL of PB buffer.

Covalent attachment of N6L pseudopeptide on BSA-NP

1 mL of activated BSA-NP at 2 mg Fe mL^{-1} was incubated with 1.1, 2.2, 4.4 or 8.8 µL of 0.62 mM Nucant-S-S-Pyr (0.4, 0.8, 1.6 or 3.2 µmol g^{-1} Fe) overnight at 37°C. After reaction, 20 µL of brine were added and the sample was centrifuged 10 min at 10000 rpm three times to eliminate any electrostatically bound N6L. From the collected supernatant the covalently immobilized Nucant onto BSA-NP was determined by quantification of the 2-pyridinethione released (λmax= 343 nm, ε343nm=8080 M cm^{-1}).

Covalent attachment of N6L pseudopeptide on BSA-NP-GEM

The remaining sulfhydryl groups of BSA-NP-GEM were reacted with the Nucant-S-S-Pyr as follows: 4 mL of activated BSA-NP-GEM at 2 mg Fe mL^{-1} was incubated with 4.35 µL of 0.62 mM Nucant-S-S-Pyr (1.5 µmol g^{-1} Fe) overnight at 37°C. After reaction, 20 µL of brine were added and the sample was centrifuged 10 min at 10000 rpm three times to eliminate any electrostatically bound N6L. From the collected supernatant the covalently immobilized Nucant onto BSA-NP-GEM was determined by quantification of the 2-pyridinethione released (λmax= 343 nm, ε343nm=8080 M cm^{-1}).

Physicochemical characterization of functionalized NP

Hydrodynamic diameter and zeta potential measurements were determined using a Zetasizer Nano-ZS device (Malvern Instruments). Hydrodynamic diameter and zeta potential were measured from dilute sample suspensions (0.1 mg Fe mL^{-1}) in water at pH 7.4 using a zeta potential cell. Ultraviolet-visible (UV-Vis) spectra were recorded on a Synergy H4 microplate reader (BioTek) using 96-well plates.

Drug release studies

The cumulative drug releases from the BSA-NP-GEM and BSA-NP-GEM-N6L were carried out under physiological conditions (pH 7.4 and 37°C) using two different concentrations of f 1,4-Dithiothreitol (DTT) as reducing agent (1µM and 1 mM of DTT to mimic the extracellular and intracellular conditions, respectively). For each experiment, 4.8 mg of BSA-NP-GEM and BSA-NP-GEM-N6L were dissolved in 1 ml of 0.01 M phosphate buffer at pH 7.4 containing either 1µM of DTT or 1 mM DTT and incubated at 37°C. The amount of GEM released was analysed at regular time intervals by High-performance liquid chromatography (HPLC) using a 1260 Infinity HPLC (Agilent Technologies) with a ZORBAX 300SB-C18 column (5µm, 9.4×250 mm), mobile phase water/acetonitrile 80/20, at flow rate of 0.3 ml min^{-1}, the absorbance was measured at 270 nm. The percentage of GEM released was calculated from a standard calibration curve of the free-drug solution.

NP sterilization

NPs were sterilized before incubation with cells. 500 µl of NP stock were dispersed by sonication for 5 min and then the NP were mixed with medium containing 10% FBS to the desired Fe concentration. The resulting sample was filtered through a 0.22 µm Millex-GP filter (Merck-Millipore Darmstadt, Germany) and sonicated again for 1 min.

Cell culture

MDA-MB-231 and MCF-10A cell lines were purchased from American Type Culture Collections (Manassas, VA, USA). MDA-MB-231 cell line was grown as monolayer in Dulbecco's Modified Eagle's Medium (DMEM) supplemented with 10% fetal bovine serum (FBS), 2 mM L-glutamine, 0.25 µg ml^{-1} fungizone, 100 units of penicillin ml^{-1} and 100 µg ml^{-1} of streptomycin. MCF-10A was grown as monolayers in human uterine microvascular endothelial cells (HuMEC) ready medium from GIBCO (HuMEC basal serum-free medium supplemented with epidermal growth factor, hydrocortisone, isoproterenol, transferrin, insulin and 25 mg of bovine pituitary extract) supplemented with 100 units of penicillin and 100 mg ml^{-1} of streptomycin (Lonza). All reagents were purchased from GIBCO. Cell lines were maintained in an incubator at 37°C in a humidified atmosphere of 95% air and 5% CO2.

In vitro cell studies

Specific targeting of breast cancer cells with BSA-NP-N6L

To determine the optimum incubation time for the specific targeting of breast cancer cell (MDA-MB-231) with BSA-NP-N6L in comparison with BSA-NP, cells were seeded at 5×10^4 cells per well in 500 µl of DMEM containing 10% FBS. After 24 hours, the growth medium was removed and cells were then incubated for 1, 2, 5 or 24 h at 37°C in the presence of BSA-NP and BSA-NP-N6L (1 µmol N6L mg^{-1} Fe, corresponding to 4 N6L per NP) at 0.2 mg Fe ml^{-1}. After incubation, cells were washed three times with phosphate-buffered saline (PBS). Prussian blue staining of iron was performed to investigate the specific binding of BSA-NP-N6L to cancer cells.

To study the effect of the number of targeting molecules per NP on the specific targeting (NP uptake) of BSA-NP-N6L for cancer cell lines (MDA-MB-231) in comparison with a non-tumorigenic cell line (MCF-10A), cells were seeded at 5×10^4

cells per well in 500 µl of DMEM containing 10% FBS or HuMEC ready medium. After 24 h, the growth medium was removed and cells were then incubated for 5 h at 37°C in the presence of BSA-NP (0 µmol N6L per mg Fe, 0 N6L per NP), BSA-NP-N6L_1 (0.25µmol N6L per mg Fe, 1 N6L per NP), BSA-NP-N6L_2 (0.5 µmol N6L per mg Fe, 2 N6L per NP), BSA-NP-N6L_3 (1 µmol N6L per mg Fe, 4 N6L per NP) and BSA-NP-N6L_4 (2 µmol N6L per mg Fe, 8 N6L per NP), at 0.2 mg Fe ml^{-1}. After incubation, cells were washed three times with phosphate-buffered saline (PBS). Finally, inductively coupled plasma mass spectrometry (ICP-MS) was performed to quantify the binding of BSA-NP-N6L to cancer cells.

Based on the results of these experiments, we selected 5 h as the optimum incubation time and 4 N6L per NP as the optimum amount of targeting agent. To verify the specific targeting of breast cancer cell (MDA-MB-231) in comparison with a non-tumorigenic cell line (MCF-10A), cells were seeded at 5×10^4 cells per well in 500 µl of DMEM containing 10% FBS or HuMEC ready medium. After 24 h, the growth medium was removed and cells were then incubated for 5 h at 37°C in the presence of BSA-NP and BSA-NP-N6L_3 (1 µmol N6L per mg Fe, 4 N6L per NP) at 0.2 mg Fe ml^{-1}. After incubation, cells were washed three times with phosphate-buffered saline (PBS). Finally, the internalization of BSA-NP and BSA-NP-N6L was assessed using confocal reflection microscopy that allows the visualization of the NPs.

Prussian blue staining

For Prussian blue staining, cells were seeded on 12 mm square glass coverslips (Maienfeld GmbH & Co.KG, Germany) placed into the wells. Briefly, the cells were washed twice with phosphate buffered saline (PBS) and fixed with 4% paraformaldehyde solution for 30 min at room temperature. The cells were then washed twice with PBS again, and subsequently incubated with a 1:1 mixture of 4% potassium ferrocyanide and 4% hydrochloric acid (Prussian blue staining solution) for 15 min at room temperature before being washed with distilled water three times. The counterstaining was done for cytoplasm with neutral red 0.5% (Panreac Química S.L.U) for 2 min at room temperature and then washed with distilled water several times. After drying the cells, the cover slips were mounted by using DePeX (SERVA Electrophoresis GmbH) and finally the cells were observed using light microscopy (Leica DMI3000B, Leica Microsystems, Germany). All experiments were carried out in triplicate. The qualitative quantification of the amount of NPs per cell form the Prussian blue experiments was performed using Image J software. Ratios between Prussian blue staining (NPs) and Phenol red staining (cells) were obtained for each image.

Inductively coupled plasma mass spectrometry (ICP-MS)

For ICP-MS, the cells were washed twice with PBS, trypsinized with 200 µl of 0.25% w/v trypsin solution and were then incubated for 5 min at 37°C. When a single cell suspension was obtained, 2 ml of complete media was added. The resultant solution was transferred to a sterile 15 ml conical centrifuge tube and centrifuged at 1200 rpm for 10 min. The supernatant was discarded carefully and cells were resuspended in 5 ml of fresh complete media and 100 µl was retained to count the cell number. The cell suspension was centrifuged again at 1200 rpm for 10 min and the supernatant was discarded carefully. 300 µl of 37% HCl was added to the cell pellet and the resultant suspension was sonicated for 30 min at 40°C. Finally, 2700 µl of bidistilled water was added and the iron concentration was determined by measuring the sample in an ICP-MS NexION 300XX (Perkin Elmer). The ICP measurements report of total Fe amount per cell (pg Fe/cell), considering that 1 pg of iron correspond to approximately 139202 NPs these values can be transform to number of NPs internalized by cell.

Confocal reflection microscopy

Cells were seeded on 12 mm square glass coverslips (Maienfeld GmbH & Co.KG, Germany) placed into the wells. Briefly, the cells were washed twice with PBS and fixed with 500 µL/well of the solution containing 4% of paraformaldehyde and 0.5% of triton X-100 for 5 minutes at room conditions followed by a second incubation during 10-15 minutes with a solution containing only 4% paraformaldehyde removing first the previous solution. Thereafter, the fixing media was removed and the cells incubated with 500 µL of DAPI 300 nM for 5 minutes covering the plates from light. Finally, cells were washed twice with PBS solution, dried at room conditions and put on microscope slides with Fluoroshield™ for observation with a TCS Leica SP5 confocal laser scanning microscope (CLSM) using a confocal reflection mode. Fluorescence images in combination with reflection (back-scattering of light by NPs) images were taken at sequential focal planes along the Z axis.

In vitro cytotoxicity assays

To assess cell death, cells (MDA-MB-231 and MCF-10A) were cultured on a 24-well plate at a density of 2.5×10^4 cells per well in 500 µl of DMEM containing 10% FBS or HuMEC ready medium. After 24 h, the growth medium was removed and cells were then incubated 5 h at 37°C in the presence of different concentrations of free GEM (1, 0.75, 0.5, 0.375 and 0.25 µM), BSA-NP-GEM and BSA-NP-GEM-N6L_3 (0.2 mg Fe ml^{-1}, 1 µM GEM; 0.15 mg Fe ml^{-1}, 0.75 µM GEM; 0.1 mg Fe ml^{-1}, 0.5 µM GEM; 0.075 mg Fe ml^{-1}, 0.375 µM GEM; 0.05 mg Fe ml^{-1}, 0.25 µM GEM). After incubation, cells were washed three times with PBS and then maintained in of DMEM containing 10% FBS or HuMEC ready medium at 37°C and 5% CO2 incubator. After 1, 2, 3 and 6 days the medium was replaced with of DMEM containing 10% FBS or HuMEC ready medium, and 10% of Resazurin dye (1 mg per ml PBS). Cells were maintained at 37°C and 5% CO2 incubator for 3 h and then, a Synergy H4 microplate reader was used to determine the amount of Resazurin by measuring the absorbance of the reaction mixture (excitation 570 nm, emission 600 nm). 600 µl of 10% of resazurin dye was added to empty wells as a negative control. The cell viability was expressed as the percentage of absorption of treated cells in comparison with control cells (without NP).

Finally, to correlate the NPs uptake with the cytotoxicity experiment, ICP-MS were performed in the same conditions that the cytotoxicity assay as follows: cells (MDA-MB-231 and MCF-10A) were cultured on a 24-well plate at a density of 2.5×10^4 cells per well in 500 µl of DMEM containing 10% FBS or HuMEC ready medium. After 24 h, the growth medium was removed and cells were then incubated 5 h at 37°C in the presence of different concentrations of BSA-NP-GEM and BSA-NP-GEM-N6L_3 (0.2 mg Fe ml^{-1}, 1 µM GEM; 0.15 mg Fe ml^{-1}, 0.75 µM GEM; 0.1 mg Fe ml^{-1}, 0.5 µM GEM; 0.075 mg Fe ml^{-1}, 0.375 µM GEM; 0.05 mg Fe ml^{-1}, 0.25 µM GEM). After incubation, cells were washed three times with PBS and then maintained in of DMEM containing 10% FBS or HuMEC ready medium at 37°C and 5% CO2 incubator. After incubation, cells were washed three times with phosphate-buffered saline (PBS). Finally, inductively coupled plasma mass spectrometry (ICP-MS) was performed to quantify the NPs uptake. All experiments were carried out in triplicate.

Acknowledgements

This work has been partially supported by Spanish Ministry of Economy and Competitiveness (BIO2012-34835, BIO2016-77367-C2-1-R to ALC and BFU2016-79127-R to RG) and Comunidad de Madrid (NANOFRONTMAG-CM, S2013/MIT- 55 2850 to ALC and AIRBIOTA-CM, S2013/MAE-2874 to RG). We thank J. Courty for the supply of N6L peptide.

Notes and references

1 B. Pelaz, C. Alexiou, R. A. Alvarez-Puebla, F. Alves, A. M. Andrews, S. Ashraf, L. P. Balogh, L. Ballerini, A. Bestetti, C. Brendel, S. Bosi, M. Carril, W. C. Chan, C. Chen, X. Chen, X. Chen, Z. Cheng, D. Cui, J. Du, C. Dullin, A. Escudero, N. Feliu, M. Gao, M. George, Y. Gogotsi, A. Grunweller, Z. Gu, N. J. Halas, N. Hampp, R. K. Hartmann, M. C. Hersam, P. Hunziker, J. Jian, X. Jiang, P. Jungebluth, P. Kadhiresan, K. Kataoka, A. Khademhosseini, J. Kopecek, N. A. Kotov, H. F. Krug, D. S. Lee, C. M. Lehr, K. W. Leong, X. J. Liang, M. Ling Lim, L. M. Liz-Marzan, X. Ma, P. Macchiarini, H. Meng, H. Mohwald, P. Mulvaney, A. E. Nel, S. Nie, P. Nordlander, T. Okano, J. Oliveira, T. H. Park, R. M. Penner, M. Prato, V. Puntes, V. M. Rotello, A. Samarakoon, R. E. Schaak, Y. Shen, S. Sjoqvist, A. G. Skirtach, M. G. Soliman, M. M. Stevens, H. W. Sung, B. Z. Tang, R. Tietze, B. N. Udugama, J. S. VanEpps, T. Weil, P. S. Weiss, I. Willner, Y. Wu, L. Yang, Z. Yue, Q. Zhang, Q. Zhang, X. E. Zhang, Y. Zhao, X. Zhou and W. J. Parak, *ACS Nano*, 2017.

2 Y. Min, J. M. Caster, M. J. Eblan and A. Z. Wang, *Chem. Rev.*, 2015, **115**, 11147-11190.

3 J. Shi, P. W. Kantoff, R. Wooster and O. C. Farokhzad, *Nature reviews. Cancer*, 2017, **17**, 20-37.

4 T. Mizuhara, D. F. Moyano and V. M. Rotello, *Nano Today*, 2016, **11**, 31-40.

5 M. E. Davis, Z. G. Chen and D. M. Shin, *Nat Rev Drug Discov*, 2008, **7**, 771-782.

6 J. Rao, *ACS Nano*, 2008, **2**, 1984-1986.

7 G. V. Dubacheva, T. Curk, R. Auzely-Velty, D. Frenkel and R. P. Richter, *Proc Natl Acad Sci U S A*, 2015, **112**, 5579-5584.

8 F. J. Martinez-Veracoechea and D. Frenkel, *Proc Natl Acad Sci U S A*, 2011, **108**, 10963-10968.

9 P. Cironi, I. A. Swinburne and P. A. Silver, *J Biol Chem*, 2008, **283**, 8469-8476.

10 V. Doldan-Martelli, R. Guantes and D. G. Miguez, *CPT Pharmacometrics Syst Pharmacol*, 2013, **2**, e26.

11 T. Ruiz-Herrero, J. Estrada, R. Guantes and D. G. Miguez, *PLoS Comput Biol*, 2013, **9**, e1003274.

12 C. B. Carlson, P. Mowery, R. M. Owen, E. C. Dykhuizen and L. L. Kiessling, *ACS Chem Biol*, 2007, **2**, 119-127.

13 S. Hong, P. R. Leroueil, I. J. Majoros, B. G. Orr, J. R. Baker, Jr. and M. M. Banaszak Holl, *Chem Biol*, 2007, **14**, 107-115.

14 D. Destouches, N. Page, Y. Hamma-Kourbali, V. Machi, O. Chaloin, S. Frechault, C. Birmpas, P. Katsoris, J. Beyrath, P. Albanese, M. Maurer, G. Carpentier, J. M. Strub, A. Van Dorsselaer, S. Muller, D. Bagnard, J. P. Briand and J. Courty, *Cancer Res.*, 2011, **71**, 3296-3305.

15 L. L. Kiessling, J. E. Gestwicki and L. E. Strong, *Curr Opin Chem Biol*, 2000, **4**, 696-703.

16 B. Sulzer and A. S. Perelson, *Math Biosci*, 1996, **135**, 147-185.

17 R. M. Fratila, S. G. Mitchell, P. del Pino, V. Grazu and J. M. de la Fuente, *Langmuir*, 2014, **30**, 15057-15071.

18 Conde J, Dias JT, Grazú V, Moros M, Baptista PV and d. l. F. JM, *Front Chem.*, 2014, **2**, 48.

19 A. Latorre, P. Couleaud, A. Aires, A. L. Cortajarena and A. Somoza, *Eur J Med Chem*, 2014, **82**, 355-362.

20 S. Hauert, S. Berman, R. Nagpal and S. N. Bhatia, *Nano Today*, 2013, **8**, 566-576.

21 S. Hauert and S. N. Bhatia, *Trends Biotechnol*, 2014, **32**, 448-455.

22 E. A. Sykes, J. Chen, G. Zheng and W. C. Chan, *ACS Nano*, 2014, **8**, 5696-5706.

23 D. Destouches, E. Huet, M. Sader, S. Frechault, G. Carpentier, F. Ayoul, J. P. Briand, S. Menashi and J. Courty, *J Biol Chem*, 2012, **287**, 43685-43693.

24 S. Kossatz, J. Grandke, P. Couleaud, A. Latorre, A. Aires, K. Crosbie-Staunton, R. Ludwig, H. Dahring, V. Ettelt, A. Lazaro-Carrillo, M. Calero, M. Sader, J. Courty, Y. Volkov, A. Prina-Mello, A. Villanueva, A. Somoza, A. L. Cortajarena, R. Miranda and I. Hilger, *Breast Cancer Res*, 2015, **17**, 66.

25 M. E. Gilles, F. Maione, M. Cossutta, G. Carpentier, L. Caruana, S. Di Maria, C. Houppe, D. Destouches, K. Shchors, C. Prochasson, F. Mongelard, S. Lamba, A. Bardelli, P. Bouvet, A. Couvelard, J. Courty, E. Giraudo and I. Cascone, *Cancer Res.*, 2016, **76**, 7181-7193.

26 M. Sader, C. P, G. Carpentier, M.-E. Gilles, N. Bousserrhine, A. Livet, I. Cascone, D. Destouches, C. AL

and J. Courty, *Nanomedicine and Nanotechnology*, 2015, **6**.

27 D. Destouches, M. Sader, S. Terry, C. Marchand, P. Maille, P. Soyeux, G. Carpentier, F. Semprez, J. Ceraline, Y. Allory, J. Courty, A. De La Taille and F. Vacherot, *Oncotarget*, 2016, **7**, 69397-69411.

28 E. Benedetti, A. Antonosante, M. d'Angelo, L. Cristiano, R. Galzio, D. Destouches, T. M. Florio, A. C. Dhez, C. Astarita, B. Cinque, A. Fidoamore, F. Rosati, M. G. Cifone, R. Ippoliti, A. Giordano, J. Courty and A. Cimini, *Oncotarget*, 2015, **6**, 42091-42104.

29 N. Jain, H. Zhu, T. Khashab, Q. Ye, B. George, R. Mathur, R. K. Singh, Z. Berkova, J. F. Wise, F. K. Braun, X. Wang, K. Patel, Z. Y. Xu-Monette, J. Courty, K. H. Young, L. Sehgal and F. Samaniego, *Leukemia*, 2017.

30 A. Aires, S. M. Ocampo, B. M. Simoes, M. Josefa Rodriguez, J. F. Cadenas, P. Couleaud, K. Spence, A. Latorre, R. Miranda, A. Somoza, R. B. Clarke, J. L. Carrascosa and A. L. Cortajarena, *Nanotechnology*, 2016, **27**, 065103.

31 A. Aires, S. M. Ocampo, D. Cabrera, L. de la Cueva, G. Salas, F.J. Teran, A.L. Cortajarena, *Journal of Materials Chemistry B*, 2015, **3**, 6239-6247.

32 B. Samanta, H. Yan, N. O. Fischer, J. Shi, D. J. Jerry and V. M. Rotello, *J Mater Chem*, 2008, **18**, 1204-1208.

33 M. C. Sader, P.; Carpentier, G.; Gilles, M.-E.; Bousserrhine, N.; Livet, A.; Cascone, I.; Destouches, D.; Cortajarena, A.L.; Courty, J., *Nanomedicine and Nanotechnology*, 2015, **6**, 1000299.

34 I. Canton and G. Battaglia, *Chem Soc Rev*, 2012, **41**, 2718-2739.

35 D. Destouches, D. El Khoury, Y. Hamma-Kourbali, B. Krust, P. Albanese, P. Katsoris, G. Guichard, J. P. Briand, J. Courty and A. G. Hovanessian, *Plos One*, 2008, **3**.

36 S. Grisendi, C. Mecucci, B. Falini and P. P. Pandolfi, *Nat Rev Cancer*, 2006, **6**, 493-505.

37 N. Afratis, C. Gialeli, D. Nikitovic, T. Tsegenidis, E. Karousou, A. D. Theocharis, M. S. Pavao, G. N. Tzanakakis and N. K. Karamanos, *Febs J*, 2012, **279**, 1177-1197.

38 D. A. Lauffenburger and J. J. Linderman, *Receptors: Models for binding, trafficking, and signaling*, Oxford University Press, New York1993.

39 T. J. Wickham, R. R. Granados, H. A. Wood, D. A. Hammer and M. L. Shuler, *Biophys J*, 1990, **58**, 1501-1516.

40 B. Sulzer and A. S. Perelson, *Mol Immunol*, 1997, **34**, 63-74.

41 B. Goldstein, J. R. Faeder and W. S. Hlavacek, *Nat Rev Immunol*, 2004, **4**, 445-456.

42 L. Treuel, X. Jiang and G. U. Nienhaus, *J R Soc Interface*, 2013, **10**, 20120939.

43 A. Verma and F. Stellacci, *Small*, 2010, **6**, 12-21.

44 M. Calero, M. Chiappi, A. Lazaro-Carrillo, M. J. Rodriguez, F. J. Chichon, K. Crosbie-Staunton, A. Prina-Mello, Y. Volkov, A. Villanueva and J. L. Carrascosa, *J Nanobiotechnology*, 2015, **13**, 16.

45 B. D. Chithrani and W. C. Chan, *Nano Lett*, 2007, **7**, 1542-1550.

46 H. Gao, W. Shi and L. B. Freund, *Proc Natl Acad Sci U S A*, 2005, **102**, 9469-9474.

47 S. Zhang, H. Gao and G. Bao, *ACS Nano*, 2015, **9**, 8655-8671.

48 Z. Cheng, A. Al Zaki, J. Z. Hui, V. R. Muzykantov and A. Tsourkas, *Science*, 2012, **338**, 903-910.

49 G. A. Kwong, J. S. Dudani, E. Carrodeguas, E. V. Mazumdar, S. M. Zekavat and S. N. Bhatia, *Proc Natl Acad Sci U S A*, 2015, **112**, 12627-12632.

50 K. A. Rejniak and A. R. Anderson, *Wiley Interdiscip Rev Syst Biol Med*, 2011, **3**, 115-125.

51 M. Robertson-Tessi, R. J. Gillies, R. A. Gatenby and A. R. Anderson, *Cancer Res*, 2015, **75**, 1567-1579.

52 Y. Qu, B. Han, Y. Yu, W. Yao, S. Bose, B. Y. Karlan, A. E. Giuliano and X. Cui, *PloS one*, 2015, **10**, e0131285.

53 A. Prina-Mello, K. Crosbie-Staunton, G. Salas, M. del Puerto Morales and Y. Volkov, *IEEE Transactions on Magnetics*, 2013, **49**, 377-382.

54 G. Salas, C. Casado, F.J. Teran, R. Miranda, C. J. S. and and M. P. Morales, *J. Mater. Chem*, 2012, **22**, 21065-21075.